Near threshold heavy quarkonium photoproduction
at large momentum transfer

Peng Sun,[1] Xuan-Bo Tong[©],[2,3] and Feng Yuan[©][4]

[1]*Department of Physics and Institute of Theoretical Physics, Nanjing Normal University,*
Nanjing, Jiangsu 210023, China
[2]*School of Science and Engineering, The Chinese University of Hong Kong,*
Shenzhen, Shenzhen, Guangdong 518172, People's Republic of China
[3]*University of Science and Technology of China, Hefei, Anhui 230026, People's Republic of China*
[4]*Nuclear Science Division, Lawrence Berkeley National Laboratory, Berkeley, California 94720, USA*

Perturbative QCD is applied to investigate the near threshold heavy quarkonium photoproduction at large momentum transfer. We take into account the contributions from the leading three-quark Fock states of the nucleon. The dominant contribution comes from the three-quark Fock state with one unit quark orbital angular momentum (OAM) whereas that from zero-quark OAM is suppressed at the threshold. From our analysis, we also show that there is no direct connection between the near threshold heavy quarkonium photoproduction and the gluonic gravitational form factors without additional approximation. Based on the comparison between our result and recent GlueX data of J/ψ photoproduction, we make predictions for ψ' and Υ (1S,2S) states which can be tested in future experiments.

I. INTRODUCTION

Exclusive heavy quarkonium production in high energy photon-proton scattering,

$$\gamma^{(*)} + N \rightarrow V + N', \tag{1}$$

where the incoming photon can be real or virtual, has attracted great attention in the hadron physics community. This process is dominated by the two-gluon exchange [1,2] and can be formulated in the generalized parton distribution (GPD) [3,4] framework [5–9]. The theory advance has also pushed the perturbative QCD computation of these processes to the next-to-leading order [9–11].

Recently, there has been a strong interest in this process at the lower end of the energy range near the threshold [12–30]. In particular, it was argued in Refs. [12,13] that this process can provide a direct access to the so-called trace anomaly contribution to the proton mass, while the origin of the proton mass is fundamental in QCD strong interaction theory [31–39].

In experiments, J/ψ photoproduction from the nuclear targets near the threshold have been investigated

before [40,41]. More recently, high-precision measurements have been carried out by the GlueX collaboration at Jefferson Lab [16]. Future experiments will explore both J/ψ and Υ near threshold photoproduction in great detail [42], including JLab-12 GeV [43,44] and electron-ion colliders [45–47].

In this paper, we will focus on one of the key aspects of the threshold kinematics that the momentum transfer is relatively large: $-t \sim 2 \text{ GeV}^2$ and 10 GeV^2 for J/ψ and Υ, respectively. Here, t is the momentum transfer squared from the nucleon target. Because of this large momentum transfer, we can apply the QCD factorization argument to compute the scattering amplitude. This factorization follows that of the hadron form factor calculations in perturbative QCD [48–55]. For the heavy quarkonium production in the final state, the nonrelativistic QCD (NRQCD) [56] will be adopted and the associated color-singlet matrix element of the quarkonium state is responsible for its production in the exclusive process.

In the perturbative calculations, the quark/gluon propagators in the scattering amplitudes lead to the power behavior for the differential cross section at large momentum transfer [57–59], which has been commonly assumed in the phenomenological studies of near threshold heavy quarkonium production; see, e.g., Refs. [16,24,25,60]. In the following, we will provide an explicit calculation to demonstrate this power behavior.

The hard exclusive processes at large momentum transfer depend on the nonperturbative distribution

amplitudes [48]. In our derivations, we take into account the contributions from the leading-twist and higher-twist terms of the nucleon distribution amplitudes [61,62]. They correspond to the three-quark Fock state light-cone wave functions of the nucleon with zero orbital angular momentum (OAM) and one-unit OAM components [63], respectively. Their contributions lead to different power behaviors at large $(-t)$, similar to the nucleon's form factors [54,55].

We will also take the heavy quark mass limit and apply the following hierarchy in scales:

$$W_{\gamma p}^2 \sim M_V^2 \gg (-t) \gg \Lambda_{\text{QCD}}^2, \qquad (2)$$

where Λ_{QCD} for the nonperturbative scale. In addition, throughout the following analysis, we take the threshold limit, i.e., $W_{\gamma p} \sim M_V + M_p$, where $W_{\gamma p}$ represents the center of mass energy and M_V and M_p for the heavy quarkonium and proton masses, respectively. To determine the leading contribution, we introduce a parameter [64],

$$\chi = \frac{M_V^2 + 2M_p M_V}{W_{\gamma p}^2 - M_p^2}, \qquad (3)$$

which goes to 1 at the threshold. We will expand the amplitude in terms of $(1 - \chi)$. By applying this expansion, we find that the commonly used $1/(-t)^4$ power term for the differential cross section is suppressed by $(1 - \chi)$. The dominant contribution at the threshold actually comes from the higher-twist term with $1/(-t)^5$ power behavior.

As mentioned above, the exclusive heavy quarkonium production has been extensively studied in the GPD framework and the scattering amplitude can be written in terms of the gluon GPDs. In Refs. [18,26,29], the GPD formalism was applied in the threshold kinematics, where the connection to the gluonic gravitational form factors was explored. In particular, the QCD factorization in terms of the gluon GPDs has been systematically argued for the threshold kinematics in Ref. [29]. One of the major objectives of this paper is to check the connection between the near threshold heavy quarkonium photoproduction and the gluonic gravitational form factors. To do that, we compare the differential cross section derived in this paper and those of the gluonic gravitational form factors of the nucleon at large momentum transfer in Ref. [55]. We will show explicitly that there is no direct connection between them without additional approximations. A brief summary of our results has been published in Ref. [65]. In the following, we provide more detailed derivations. In addition, we will compare our result to the GPD formalism and show explicitly that they are consistent with each other. A simpler process of near threshold photoproduction on the pion target will be demonstrated as well. All these derivations will help to build a solid foundation to study nucleon structure through near threshold heavy quarkonium photoproduction.

The rest of the paper is organized as follows. In Sec. II, we will examine the threshold kinematics and apply the expansion method mentioned above to simplify the derivation. In Sec. III, we take the example of photon scattering off a pion target. The leading Fock state of the pion contains quark and antiquark and the derivation is much simpler compared to the nucleon case. Sections IV and V will be dedicated to the nucleon case. In Sec. IV, we study the contribution from the leading component of the nucleon distribution amplitude and show that its contribution is actually suppressed in the threshold limit. In Sec. V, we perform the analysis of higher-twist component of the nucleon distribution amplitude and show that its contribution to the differential cross section does not vanish at the threshold. In Sec. VI, we discuss the interpretation and consequence of our derivations. We conclude that there is no direct connection between the near threshold photoproduction of heavy quarkonium and the gluonic gravitational form factors of the nucleon. In Sec. VII, we provide phenomenological applications of our derivations. Predictions on ψ' and Υ will be presented for future experiments based on the comparison between our results and the GlueX data on near threshold J/ψ production at JLab. Finally, we summarize our paper in Sec. VIII.

II. NEAR THRESHOLD KINEMATICS

The typical Feynman diagram of the two-gluon exchange contributions to the near threshold heavy quarkonium photoproduction is shown in Fig. 1,

$$\gamma(k_\gamma) + N(p_1) \to J/\psi(k_\psi) + N'(p_2), \qquad (4)$$

where we have used J/ψ as an example. In order to make the near threshold expansion more evident, it is useful to examine the relevant kinematics for the scattering amplitude. The center of mass energy and momentum transfer squared can be written as

$$W_{\gamma p}^2 = (k_\gamma + p_1)^2 = (k_\psi + p_2)^2 \sim M_V^2, \qquad (5)$$

$$|t| = |(p_2 - p_1)^2| \ll M_V^2. \qquad (6)$$

Therefore, we will have the following approximations around the threshold kinematics:
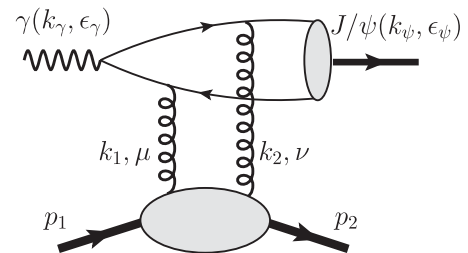

FIG. 1. Schematics of two-gluon exchange contribution to the threshold heavy quarkonium production.

$$p_1 \cdot k_\gamma \sim p_1 \cdot k_\psi \sim M_V^2, \tag{7}$$

$$p_2 \cdot k_\gamma \sim p_2 \cdot k_\psi \ll M_V^2. \tag{8}$$

In addition, applying the heavy quark mass limit of $M_V^2 \gg (-t)$, we find that the invariant mass of the t-channel two gluons is much smaller than heavy quarkonium mass. We will also take the approximation of $M_c \approx M_V/2$ in the nonrelativistic limit of the heavy quarkonium system.

The quark propagators in the upper part of the Feynman diagram of Fig. 1 are all in order of $1/M_V$. For example, one of the quark propagators can be simplified as

$$\frac{1}{(k_1 - k_\psi/2)^2 - M_c^2} = \frac{1}{-k_1 \cdot k_\gamma - k_1 \cdot k_2}$$
$$\approx \frac{1}{-k_1 \cdot k_\gamma}, \tag{9}$$

where we have applied $|k_1^2| \sim |k_2^2| \sim |k_1 \cdot k_2| \sim |t| \ll M_V^2$. Because k_1 carries certain momentum fraction of the incoming nucleon, $k_1 \cdot k_\gamma$ will be order of M_V^2. Similarly, we have

$$\frac{1}{(k_2 - k_\psi/2)^2 - M_c^2} \approx \frac{1}{-k_2 \cdot k_\gamma}. \tag{10}$$

The following propagator will also show up in some of the Feynman diagrams:

$$\frac{1}{(k - k_\psi/2)^2 - M_c^2} = \frac{1}{-k \cdot k_\gamma} \approx \frac{2}{-M_V^2}, \tag{11}$$

where $k = k_1 + k_2 = p_1 - p_2$. In the center of mass frame, k is dominated by p_1 because p_2 is soft.

Applying the above approximations, we can simplify the photon-heavy quarkonium transition amplitude. Let us define μ and ν for the polarization indices for k_1 and k_2, respectively, and ϵ_γ and ϵ_ψ for the photon polarization and J/ψ polarization vectors, respectively. To further simplify the derivation, we choose the physical polarization for the incoming photon,

$$\epsilon_\gamma \cdot k_\gamma = 0, \qquad \epsilon_\gamma \cdot p_1 = 0. \tag{12}$$

With this choice, we notice that the contributions from $\epsilon_\gamma \cdot k_1$ and $\epsilon_\gamma \cdot k_2$ are also suppressed in the heavy quark mass limit. Therefore, we will drop these terms as well. We emphasize, all these approximations have been cross-checked by a full computation.

Finally, we have the following expression for the amplitude from the heavy quarkonium side:

$$\mathcal{M}_{\psi,ab}^{\mu\nu} = \frac{\delta^{ab} N_\psi [\epsilon_\psi^* \cdot \epsilon_\gamma \mathcal{W}_T^{\mu\nu} + \epsilon_\psi^* \cdot k \mathcal{W}_L^{\mu\nu} + \mathcal{W}_S^{\mu\nu}]}{k_1 \cdot k_\gamma k_2 \cdot k_\gamma}, \tag{13}$$

where a and b represent the color indices for the t-channel gluons. In the above equation, N_ψ is defined as

$$N_\psi = -\frac{4e_c e g_s^2}{\sqrt{N_c M_V^3}} \psi_J(0), \tag{14}$$

where $\psi_J(0)$ is the wave function of J/ψ at the origin and is related to the NRQCD matrix element [56]. The tensor structures $\mathcal{W}_{T,L,S}^{\mu\nu}$ are defined as

$$\begin{aligned}
\mathcal{W}_T^{\mu\nu} &= -k_1 \cdot k_\gamma k_2 \cdot k_\gamma g^{\mu\nu} - k_1 \cdot k_2 k_\gamma^\mu k_\gamma^\nu \\
&\quad + k_1 \cdot k_\gamma k_2^\mu k_\gamma^\nu + k_2 \cdot k_\gamma k_1^\nu k_\gamma^\mu \\
\mathcal{W}_L^{\mu\nu} &= k_1 \cdot k_\gamma \epsilon_\gamma^\nu k_2^\mu + k_2 \cdot k_\gamma \epsilon_\gamma^\mu k_1^\nu \\
\mathcal{W}_S^{\mu\nu} &= -k_1 \cdot k_2 (k_1 \cdot k_\gamma \epsilon_\psi^{*\mu} \epsilon_\gamma^\nu + k_2 \cdot k_\gamma \epsilon_\psi^{*\nu} \epsilon_\gamma^\mu \\
&\quad + k_1 \cdot \epsilon_\psi^* k_\gamma^\nu \epsilon_\gamma^\mu + k_2 \cdot \epsilon_\psi^* k_\gamma^\mu \epsilon_\gamma^\nu),
\end{aligned} \tag{15}$$

where $\mathcal{W}_T$ and $\mathcal{W}_L$ represent the amplitudes for a transversely polarized and longitudinal polarized heavy quarkonium in the final state, respectively, whereas $\mathcal{W}_S$ for a subleading term.

Clearly the above amplitude is symmetric under $k_1, \mu \leftrightarrow k_2, \nu$. In the above equation, the first term is the leading contribution in the heavy quark mass limit at the threshold. The second and third terms are subleading contributions.

We have also carried out an important cross-check for the above results. We compute the full amplitude without any approximation. We then take the leading contribution of the differential cross section (the amplitude squared) in the heavy quark mass limit and threshold limit, and obtain the same result.

A. Vanishing of three-gluon exchange contribution

Before we start our derivations of the threshold scattering amplitudes, we would like to comment on the three-gluon exchange contributions. The two-gluon and three-gluon exchange diagrams were considered in Ref. [64] for the threshold production of J/ψ and it was argued that the three-gluon exchange diagrams dominate the differential cross-section contributions.

However, we find that the three-gluon exchange diagrams do not contribute in our framework, due to the C-parity conservation. This is because the three gluons from the nucleon side carry symmetric color structure (such as d_{abc}) while those from the heavy quarkonium (J/ψ) side are antisymmetric (such as f_{abc}), where a, b, and c represent the color indices for the three gluons in the t channel, respectively. Explicitly, from the nucleon side, we have, as shown in Fig. 2,

$$\epsilon^{ijk} \epsilon^{lmn} T_{il}^a T_{jm}^b T_{kn}^c \propto d^{abc}, \tag{16}$$

where ijk and lmn represent the color indices for the initial and final three quarks, respectively. Here, we have applied
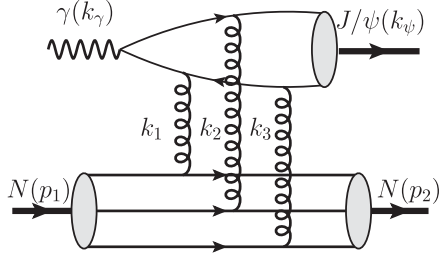
FIG. 2. Typical Feynman diagram from three-gluon exchange. These diagrams vanish because of the C-parity conservation.

the antisymmetric color structure for the three-quark Fock state wave function of the nucleon [63]. On the other hand, for the heavy quarkonium side, we have, instead

$$\mathrm{Tr}[T^a T^b T^c] = \frac{1}{4}(d^{abc} + if^{abc}).\tag{17}$$

However, because J/ψ is in the 1^{--} state, the photon-J/ψ transition amplitude vanishes for the symmetric color configuration with three gluons, i.e., d^{abc} term from the above vanishes. Combining this with the color structure from the nucleon side, we conclude the three-gluon exchange diagrams do not contribute.

III. PION CASE

In this section, we take the example of pion case to show the details of our derivations. In this case, we have photon scatters on the pion target and it produces a J/ψ in the final state close to the threshold,

$$\gamma + \pi \to J/\psi + \pi,\tag{18}$$

where the dominant contribution is again a two-gluon exchange diagram. The two gluons attach to the two quark lines from the pion target, as shown in Fig. 3.

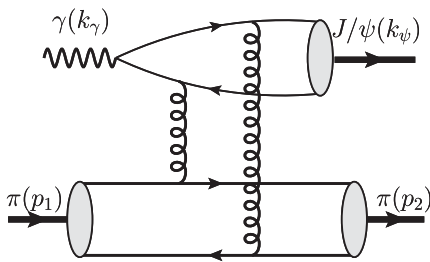Considering the leading Fock component of the pion, we have

FIG. 3. The Feynman diagram contribution to the exclusive $\gamma\pi \to \pi J/\psi$ at large momentum transfer. The two gluons attach to the quark and antiquark lines, respectively.

$$|\pi^+\rangle_{u\bar{d}} = \int d[1]d[2]\psi_{u\bar{d}}(1,2)\frac{\delta_{ij}}{\sqrt{3}}[u^\dagger_{\uparrow i}(1)\bar{d}^\dagger_{\downarrow j}(2) \\ - u^\dagger_{\downarrow i}(1)\bar{d}^\dagger_{\uparrow j}(2)]|0\rangle,\tag{19}$$

where i and $j = 1, 2, 3$ are the color indices, and $\uparrow$ and $\downarrow$ label quark light-cone helicity $+1/2$ and $-1/2$, respectively. The color factor $\delta_{ij}/\sqrt{3}$ is normalized to 1. The light-cone wave-function amplitude $\psi_{u\bar{d}}(1,2)$ is a function of quark momenta with argument 1 representing x_1 and $q_{1\perp}$ and so on. Since the momentum conservation implies $\vec{q}_{1\perp} + \vec{q}_{2\perp} = 0$ and $x_1 + x_2 = 1$, $\psi_{u\bar{d}}(1,2)$ depends on variables x_1 and $q_{1\perp}$ only. The integration in the above equation is defined as

$$\int d[1]d[2] = \int \frac{d^2 q_{1\perp}}{(2\pi)^3} \frac{dx_1}{2\sqrt{x_1(1-x_1)}}.\tag{20}$$

From the light-cone wave function, we obtain the distribution amplitude:

$$\phi(x) = \int \frac{d^2 q_{1\perp}}{(2\pi)^3} \psi_{u\bar{d}}(1,2).\tag{21}$$

The final scattering amplitude of $\gamma + \pi^+ \to J/\psi + \pi^+$ can be computed in terms of the above distribution amplitude of pion,

$$\mathcal{A}^\pi = \int dx_1 dy_1 \phi^*(y_1)\phi(x_1)\mathcal{M}^{\mu\nu}_\psi(\epsilon_\gamma, \epsilon_\psi, x_1, y_1) \\ \times \frac{-g_s^2 C_F}{2k_1^2 k_2^2}\mathrm{Tr}[\not{p}_2\gamma^\mu\not{p}_1\gamma^\nu],\tag{22}$$

where $\mathcal{M}^{\mu\nu}_\psi$ has been given in the previous section.

A. Threshold expansion

At the threshold, the amplitude squared can be further simplified as

$$|\overline{\mathcal{A}^\pi}|^2 = G_\psi G_\pi(t)G_\pi^*(t),\tag{23}$$

where the spin sum and average have been applied. Here, G_ψ is defined as

$$G_\psi = |N_\psi|^2 = \frac{384\pi^2 e_c^2\alpha(4\pi\alpha_s)^2}{N_c^2 M_\psi^3}\langle 0|\mathcal{O}^\psi(^3S_1^{(1)})|0\rangle,\tag{24}$$

where $\langle 0|\mathcal{O}(^3S_1)|0\rangle$ is the color-singlet NRQCD matrix element for J/ψ. $G_\pi(t)$ is defined as

$$G_\pi(t) = \frac{8\pi\alpha_s C_F}{t}\int dx_1 dy_1 \phi^*(y_1)\phi(x_1)\frac{1}{x_1\bar{x}_1 y_1\bar{y}_1},\tag{25}$$

where $C_F = (N_c^2 - 1)/2N_c$, $\bar{x}_1 = 1 - x_1$, and $\bar{y}_1 = 1 - y_1$. Here, we have neglected high-order corrections of $t_\psi = -t/M_V^2$.

B. Comparison to the gravitational form factors

We now compare the above result to the gluonic gravitational form factors at large momentum transfer, which have been computed in Ref. [55]. For convenience, we list the results below. The gluonic gravitation form factors of the pion are defined as

$$
\langle p_2 | T_g^{\mu\nu} | p_1 \rangle = 2\bar{P}^\mu \bar{P}^\nu A_g^\pi(t) + \frac{1}{2}(\Delta^\mu \Delta^\nu - g^{\mu\nu}\Delta^2)C_g^\pi(t)
$$
$$
+ 2m^2 g^{\mu\nu}\bar{C}_g^\pi(t), \tag{26}
$$

where $T_g^{\mu\nu}$ is the gluonic energy-momentum tensor in QCD and m represents the pion mass. Here, $\bar{P} = (p_1 + p_2)/2$ is the average momentum, $\Delta = p_2 - p_1$ is the momentum transfer, and hence $t = \Delta^2$. From the results of Ref. [55], we find

$$
A_g^\pi(t) = C_g^\pi(t) = \frac{4m^2}{t}\bar{C}_g^\pi(t)
$$
$$
= \frac{4\pi\alpha_s C_F}{-t} \int dx_1 dy_1 \phi^*(y_1)\phi(x_1)\left(\frac{1}{x_1\bar{x}_1} + \frac{1}{y_1\bar{y}_1}\right). \tag{27}
$$

From the above results, we find that there is no direct connection between $G_\pi(t)$ of Eq. (25) and any of the gravitational form factors of $A_g^\pi(t)$, $C_g^\pi(t)$, or $\bar{C}_g^\pi(t)$ [Eq. (27)]. This indicates that we cannot directly interpret the near threshold heavy quarkonium photoproduction in terms of the gluonic gravitational form factors.

C. Comparison to the GPD formalism

As mentioned in the Introduction, the photoproduction of heavy quarkonium has been derived in the GPD framework. If we extend these derivations to the near threshold kinematics, we obtain

$$
\mathcal{A}^\pi = N_\psi \epsilon_\psi^* \cdot \epsilon_\gamma \int_{-1}^{1} dx \frac{H_g^\pi(x, \xi, t)}{(x + \xi - i\epsilon)(x - \xi + i\epsilon)} \tag{28}
$$

for the pion target, where N_ψ has been given in Eq. (14) and ξ is the skewness parameter. In the threshold limit we take $\xi = 1$. In the above equation, H_g^π represents the GPD gluon distribution of the pion. The GPD gluon distribution at large momentum transfer can be calculated in terms of the distribution amplitudes as that of the quark GPD in Ref. [66], which we list in Appendix A. If we substitute the result of $H_g^\pi(x, \xi, t)$ from there, we will be able to reproduce the scattering amplitude result from the direct computation in the above subsection III A. This provides a useful cross-check for our derivations.

IV. NUCLEON CASE: TWIST-THREE CONTRIBUTIONS

Now we turn to the proton cases. We show the typical Feynman diagram in Fig. 4. To compute these diagrams, we follow the factorization argument for the hard exclusive processes [49], where the leading contributions come from the three-quark Fock state of the nucleon. The three-quark states can be further classified into zero orbital angular momentum (OAM) and nonzero OAM components [63]. We will first examine the contribution from zero OAM component. This corresponds to the twist-three contribution from the nucleon's distribution amplitude.

A. Three-quark Fock state with zero OAM

Because there is no quark OAM, the total quark spin equals to the nucleon spin. The associated light-cone wavefunction amplitude is defined as

$$
|P\uparrow\rangle_{1/2} = \int d[1]d[2]d[3](\tilde{\psi}^{(1)}(1,2,3))
$$
$$
\times \frac{\epsilon^{ijk}}{\sqrt{6}} u_{i\uparrow}^\dagger(1)(u_{j\downarrow}^\dagger(2)d_{k\uparrow}^\dagger(3) - d_{j\downarrow}^\dagger(2)u_{k\uparrow}^\dagger(3))|0\rangle, \tag{29}
$$

where ijk represent the color indices for the three quarks, respectively, and the measure for the quark momentum is

$$
d[1]d[2]d[3] = \sqrt{2}\frac{dx_1 dx_2 dx_3}{\sqrt{2x_1 2x_2 2x_3}}\frac{d^2\vec{q}_{1\perp}d^2\vec{q}_{2\perp}d^2\vec{q}_{3\perp}}{(2\pi)^9}
$$
$$
\times (2\pi)^3\delta(1 - x_1 - x_2 - x_3)
$$
$$
\times \delta^{(2)}(\vec{q}_{1\perp} + \vec{q}_{2\perp} + \vec{q}_{3\perp}). \tag{30}
$$

By integrating over the transverse momenta $q_{i\perp}$, we obtain the twist-three distribution amplitude [61]:

$$
\Phi_3(x_1, x_2, x_3) = -2\sqrt{6}\int [dq_\perp]\tilde{\psi}^{(1)}(1,2,3), \tag{31}
$$

where $[dq_\perp] = \frac{d^2\vec{q}_{1\perp}d^2\vec{q}_{2\perp}d^2\vec{q}_{3\perp}}{(2\pi)^9}\delta^{(2)}(\vec{q}_{1\perp} + \vec{q}_{2\perp} + \vec{q}_{3\perp})$. In this configuration, the three quarks only carry longitudinal
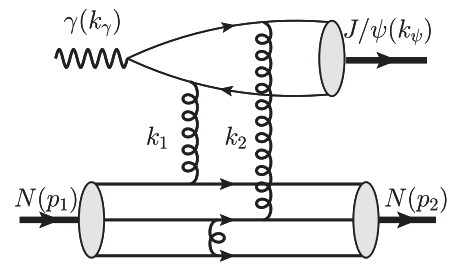

FIG. 4. Typical Feynman diagram contributions to the threshold J/ψ photoproduction at large momentum transfer from two-gluon exchange.

momenta to form the nucleon state. The above paramet-rization applies to both initial and final-state nucleons. Of course, their momenta are different. In addition, because the quark helicities are conserved, the nucleon helicity is also conserved.

B. Partonic scattering amplitude

Schematically, we can write the helicity-conserved amplitude as

$$
\mathcal{A}_3 = \langle J/\psi(\epsilon_\psi), N'_\uparrow | \gamma(\epsilon_\gamma), N_\uparrow \rangle
$$

$$
= \int [dx][dy] \Phi(x_1, x_2, x_3) \Phi^*(y_1, y_2, y_3)
$$

$$
\times \mathcal{M}^{\mu\nu}_\psi(\epsilon_\gamma, \epsilon_\psi) \frac{1}{(-t)^2} \mathcal{H}^{\mu\nu}(\{x\}, \{y\}), \qquad (32)
$$

where $\{x\} = (x_1, x_2, x_3)$ represent the momentum frac-tions carried by the three quarks, $[dx] = dx_1 dx_2 dx_3 \delta \times (1 - x_1 - x_2 - x_3)$, and $\Phi_3(x_1, x_2, x_3)$ is the twist-three distribution amplitude of the proton [61,67]. The partonic amplitude $\mathcal{H}^{\mu\nu}$ is calculated from the lower part of Fig. 4, where the incoming three quarks carry momenta of $x_1 p_1$, $x_2 p_1$, and $x_3 p_1$ and outgoing quarks with momenta of $y_1 p_2$, $y_2 p_2$, and $y_3 p_2$, respectively.

There are a total of 12 diagrams (lower part) for the $\mathcal{H}^{\mu\nu}$. However, all the diagrams can be generated by only two specific diagrams with different helicity configurations and arrangement (permutation) of the momenta for the quark lines. First, all these diagrams have the same color factor,

$$
C_B^2 \equiv \delta^{ac} \frac{1}{6} \epsilon_{ijk} \epsilon_{i'j'k'} (T^a)_{i'i} (T^c T^b)_{j'j} (T^b)_{k'k}
$$

$$
= \left(\frac{2}{3}\right)^2. \qquad (33)
$$

For these diagrams, a pair of quarks has zero total helicity. One can combine these two fermion lines into a Dirac trace, by applying the following identity:

$$
\bar{U}_{\uparrow/\downarrow}(p_2) \Gamma U_{\uparrow/\downarrow}(p_1) = \bar{U}_{\downarrow/\uparrow}(p_1) \Gamma_R U_{\downarrow/\uparrow}(p_2), \qquad (34)
$$

where Γ_R is a γ-matrix chain obtained by reversing the order in Γ. This leads to the typical Dirac algebra for the partonic amplitude $\mathcal{H}^{\mu\nu}$,

$$
\bar{U}_\uparrow(p_2) \Gamma_1 U_\uparrow(p_1) \bar{U}_\uparrow(p_1) \Gamma_{2R} U_\uparrow(p_2) \bar{U}_\uparrow(p_2) \Gamma_3 U_\uparrow(p_1). \qquad (35)
$$

It is easy to find that the first two factors can be combined into a Dirac trace, and we obtain the following expression:
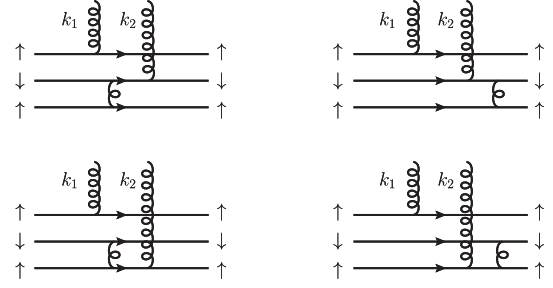

FIG. 5. Partonic scattering amplitude for the type I configura-tion: k_1 is determined by the quark line with helicity-up state.

$$
\text{Tr}\left[\frac{1 + \gamma_5}{2} \not{p}_2 \Gamma_1 \frac{1 + \gamma_5}{2} \not{p}_1 \Gamma_{2R} \right] \bar{U}_\uparrow(p_2) \Gamma_3 U_\uparrow(p_1). \qquad (36)
$$

We will apply the above simplification to all the diagrams.

Furthermore, by examining the two gluon kinematics, we realize that one of the gluons' kinematics is determined completely by the quark line to which the gluon attaches. Let us identify that gluon as "k_1." Therefore, $k_1 = x_i p_1 - y_i p_2$, where i represents the quark line in the diagram. With k_1 determined, we immediately deduce that $k_2 = \bar{x}_i p_1 - \bar{y}_i p_2$.

Therefore, we can classify the partonic scattering ampli-tudes into two groups: $k_1 = x_i p_1 - y_i p_2$ attaches to the helicity-up quark line (type I) and k_1 attaches to the helcity-down quark line (type II). The derivations for both types are similar but differ in some details.

The typical diagrams of type I are shown in Fig. 5, where we include all possible attachments of k_2 and the additional gluon exchange between the two quark lines. The con-tributions of all these four diagrams can be evaluated at the same time and will be grouped together. For these diagrams, it is easy to show that the amplitude can be written as

$$
\bar{U}_\uparrow(p_2) \gamma^\mu U_\uparrow(p_1) \text{Tr}\left[\frac{1 + \gamma_5}{2} \not{p}_2 \cdots \gamma^\nu \cdots \frac{1 + \gamma_5}{2} \not{p}_1 \cdots \right].
$$
$$
\qquad (37)
$$

Because there is no other vector than p_1, p_2, and ν, we conclude that the trace of the second factor is proportional to p_1^ν or p_2^ν. Explicitly, these four diagrams contribute

$$
\frac{p_2^\nu}{x_3 y_3 \bar{x}_1}, \qquad \frac{p_1^\nu}{x_3 y_3 \bar{y}_1}, \qquad \frac{p_2^\nu}{x_2 y_2 \bar{x}_1}, \qquad \frac{p_1^\nu}{x_2 y_2 \bar{y}_1}. \qquad (38)
$$

Adding them together, we have

$$
\frac{1}{x_1 y_1 \bar{x}_1 \bar{y}_1} \left(\frac{1}{x_2 y_2} + \frac{1}{x_3 y_3} \right) \frac{\bar{x}_1 p_1^\nu + \bar{y}_1 p_2^\nu}{\bar{x}_1 \bar{y}_1}, \qquad (39)
$$

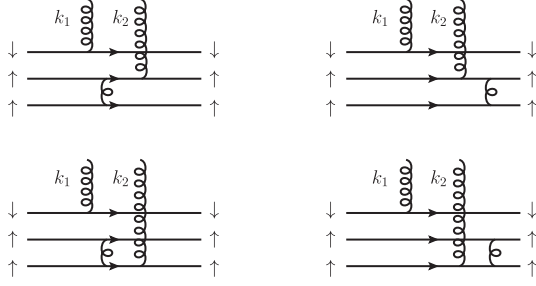where we have also included the t-channel gluon propagators.

FIG. 6.   Partonic scattering amplitude for the type-II configuration: k_1 is determined by the quark line with helicity-down state.

Typical type-II diagrams are shown in Fig. 6. The calculations are a little bit involved. For example, the amplitude can be written in the following form:

$$\bar{U}_\uparrow(p_2)\gamma^\rho U_\uparrow(p_1)\text{Tr}\left[\frac{1+\gamma_5}{2}\not{p}_2\cdots\gamma^\nu\cdots\frac{1+\gamma_5}{2}\not{p}_1\cdots\gamma_\rho\cdots\right].$$

(40)

Now the trace of the Gamma matrices can lead to a term like $\epsilon^{p_1 p_2 \nu \rho}$, which can be simplified by applying the following identity:

$$\bar{U}_\uparrow(p_2)\gamma^\mu U_\uparrow(p_1) = \frac{i\epsilon^{\mu\nu p_1 p_2}}{p_1\cdot p_2}\bar{U}_\uparrow(p_2)\gamma_\nu U_\uparrow(p_1).$$

(41)

In the end, we find that there is cancellation between different terms and the type-II diagrams vanish.

To derive the final result for the amplitude, we need to contract the $\mathcal{M}^{\mu\nu}$ with $\mathcal{H}^{\mu\nu}$ in Eq. (32). The final results can be summarized as

$$\mathcal{A}_3 = \langle J/\psi(\epsilon_\psi), N'_\uparrow|\gamma(\epsilon_\gamma), N_\uparrow\rangle$$
$$= \int[dx][dy]\Phi(x_1,x_2,x_3)\Phi^*(y_1,y_2,y_3)\frac{1}{(-t)^2}$$
$$\times \bar{U}_\uparrow(p_2)\not{k}_\gamma U_\uparrow(p_1)\mathcal{M}^{(3)}(\epsilon_\gamma,\epsilon_\psi,\{x\},\{y\}).$$

(42)

The spinor structure in the above equation is a consequence of the leading-twist amplitude which conserves the nucleon helicity. This is similar to the A form-factor calculation in Ref. [55].

C. Threshold expansion

In the threshold limit, we find that $\mathcal{M}^{(3)}$ can be further simplified as

$$\mathcal{M}^{(3)} = \epsilon_\psi^* \cdot \epsilon_\gamma \frac{8e_c e g_s^6}{27\sqrt{3M_\psi^7}}\psi_J(0)(2\mathcal{H}_3+\mathcal{H}'_3).$$

(43)

The coefficient $\mathcal{H}_3$ can be summarized as

$$\mathcal{H}_3 = I_{13}+I_{31}+I_{12}+I_{32},$$

(44)

where

$$I_{ij} = \frac{1}{x_i x_j y_i y_j \bar{x}_i^2 \bar{y}_i}$$

(45)

and $\mathcal{H}'_3 = \mathcal{H}_3(y_1 \leftrightarrow y_3)$.

Similar to the pion case, we can reproduce the above result by applying the GPD gluon distribution $H_g(x,\xi,t)$ at large momentum transfer in the GPD formalism. For reference, we list the GPD gluon distribution H_g in Appendix B.

The final result for the differential cross section will depend on the threshold limit of the amplitude squared. In the limit of $\chi \to 1$ we find the following result:

$$|\overline{\mathcal{A}_3}|^2 = (1-\chi)G_\psi G_{p3}(t)G^*_{p3}(t),$$

(46)

which actually vanishes at the threshold. In the above, the spin sum and average has been performed, and G_ψ has been defined in Eq. (24). G_{p3} follows the form-factor factorization and can be written as

$$G_{p3}(t) = \frac{8\pi^2\alpha_s^2 C_B^2}{3t^2}\int[dx][dy]\Phi_3(\{x\})\Phi_3^*(\{y\})[2\mathcal{H}_3+\mathcal{H}'_3],$$

(47)

where $\mathcal{H}_3$ and $\mathcal{H}'_3$ are given above, and $C_B^2 = (2/3)^2$ is the color factor related to partonic amplitudes. Combining G_{p3} and G^*_{p3}, this leads to $1/(-t)^4$ power behavior for the amplitude squared, which is consistent with the conventional power counting analysis. However, this contribution is suppressed at the threshold.

The suppression factor $(1-\chi)$ comes from the spinor structure in Eq. (42). In order to obtain a nonvanishing contribution at the threshold, we have to go beyond the leading-twist contributions. In the following section, we consider the three-quark Fock states with one-unit OAM, which are related to the twist-four distribution amplitudes [61,63].

V. NUCLEON CASE: TWIST-FOUR CONTRIBUTIONS

The twist-four contribution comes from the three-quark Fock state with one unit quark OAM. Two important features emerge for nonzero OAM contributions. First, the partonic scattering amplitudes conserve the quark helicities. However, because of a nonzero OAM for one of the three-quark states, the helicity of the nucleon states will be different. This contributes to the hadron helicity-flip amplitude. Second, in order to get a nonzero contribution, we have to perform the intrinsic transverse momentum

expansion for the hard partonic scattering amplitudes [54], which will introduce an additional suppression factor of $1/(-t)$.

The twist-four distribution amplitudes are related to the three-quark Fock states with one unit of OAM. This can comes from either the initial or final state. For example, if we consider the contribution from the initial state of spin-down nucleon, we can parametrize the Fock state as [63]

$$
\begin{aligned}
|p_1\downarrow\rangle_{1/2} = \int & d[1]d[2]d[3]((q_1^x - iq_1^y)\tilde{\psi}^{(3)}(1,2,3) \\
& + (q_2^x - iq_2^y)\tilde{\psi}^{(4)}(1,2,3))\frac{\epsilon^{ijk}}{\sqrt{6}} \\
& \times (u_{i\downarrow}^\dagger(1)u_{j\uparrow}^\dagger(2)d_{k\uparrow}^\dagger(3) - d_{i\downarrow}^\dagger(1)u_{j\uparrow}^\dagger(2)u_{k\uparrow}^\dagger(3))|0\rangle,
\end{aligned}
$$

where the total quark helicity equals $+1/2$ with nucleon helicity $-1/2$. With this choice, the final-state nucleon's Fock state can be taken as that in the previous section.

An important step in the computation of twist-four contribution is to perform the collinear expansion of the partonic scattering amplitude in terms of the transverse momenta $q_{i\perp}$. In particular, the linear term of $q_{i\perp}$ will lead to the twist-four distribution amplitudes when we integrate over the $q_{i\perp}$ [54],

$$
\begin{aligned}
\Psi_4(x_1, x_2, x_3) = -\frac{2\sqrt{6}}{x_2 M} \int & [dq_\perp]\vec{q}_{2\perp} \\
& \cdot [\vec{q}_{1\perp}\tilde{\psi}^{(3)}(1,2,3) + \vec{q}_{2\perp}\tilde{\psi}^{(4)}(1,2,3)],
\end{aligned}
\tag{48}
$$

$$
\begin{aligned}
\Phi_4(x_2, x_1, x_3) = -\frac{2\sqrt{6}}{x_3 M} \int & [dq_\perp]\vec{q}_{3\perp} \\
& \cdot [\vec{q}_{1\perp}\tilde{\psi}^{(3)}(1,2,3) + \vec{q}_{2\perp}\tilde{\psi}^{(4)}(1,2,3)].
\end{aligned}
\tag{49}
$$

To extract the linear dependence of the transverse momentum $q_{i\perp}$ from the partonic amplitudes, one can first expand the spinor as

$$
U(x_i p_1 + \vec{q}_{i\perp}) \approx U(x_i p_1) + \frac{\vec{q}_{i\perp}\not{p}_2}{2x_i p_2 \cdot p_1}U(x_i p_1). \tag{50}
$$

After the evaluation of the Dirac structures in the amplitudes following the strategy in the last section, all the linear dependence of $\vec{q}_i$ is explicit and straightforward to find. For the contributions associated with the initial OAM, it will yield a structure like

$$
\begin{aligned}
\Gamma_1(\{x\}, \{y\})(q_1^x + iq_1^y)\bar{U}_\uparrow(p_2)U_\downarrow(p_1) + \Gamma_3(\{x\}, \{y\})(q_3^x \\
+ iq_3^y)\bar{U}_\uparrow(p_2)U_\downarrow(p_1),
\end{aligned}
\tag{51}
$$

where the transverse momentum conservation $\vec{q}_{2\perp} = -\vec{q}_{1\perp} - \vec{q}_{3\perp}$ is used, and the identities $\gamma^x U_\uparrow(p) = U_\downarrow(p)$, $\gamma^y U_\uparrow(p) = iU_\downarrow(p)$ have been applied.

Applying Eqs. (48) and (49) with the linear terms of $q_{i\perp}$ from the partonic amplitudes, we obtain the twist-four contribution to the scattering process of $\gamma p \to J/\psi p$ as

$$
\begin{aligned}
\mathcal{A}_4 &= \langle J/\psi(\epsilon_\psi), N'_\uparrow|\gamma(\epsilon_\gamma), N_\downarrow\rangle \\
&= \bar{U}_\uparrow(p_2)U_\downarrow(p_1)\frac{M_p}{(-t)^3}\int[dx][dy]\Phi_3^*(\{y\}) \\
&\quad \times [\Psi_4(\{x\})\mathcal{M}_\Psi^{(4)} + \Phi_4(\{x\})\mathcal{M}_\Phi^{(4)}],
\end{aligned}
\tag{52}
$$

where Ψ_4 and Φ_4 are the twist-four distributions introduced above and $\mathcal{M}_{\Psi,\Phi}^{(4)}$ from the partonic amplitudes. From this equation, we can clearly see that the nucleon helicity flip is manifest in the spinor structure. This amplitude is negligible at high energy, but will be important at the threshold, because it is not suppressed in the limit of $\chi \to 1$. The amplitude squared along with the associated spin sum and average can be written as

$$
|\overline{\mathcal{A}_4}|^2 = \tilde{m}_t^2 G_\psi G_{p4}(t)G_{p4}^*(t), \tag{53}
$$

where $\tilde{m}_t^2 = M_p^2/(-t)$, G_ψ is the same as above. G_{p4} depends on the twist-three and twist-four distribution amplitudes [61,62],

$$
\begin{aligned}
G_{p4}(t) = \frac{C_B^2(4\pi\alpha_s)^2}{12t^2}\int & [dx][dy]\Phi_3(y_1, y_2, y_3) \\
& \times \{x_3\Phi_4(x_1, x_2, x_3)T_{4\Phi}(\{x\}, \{y\}) \\
& + x_1\Psi_4(x_2, x_1, x_3)T_{4\Psi}(\{x\}, \{y\})\},
\end{aligned}
\tag{54}
$$

where the hard function has the following form:

$$
\begin{aligned}
T_{4\Psi} &= 2\mathcal{T}_{4\Psi} + \mathcal{T}'_{4\Psi}, \\
T_{4\Phi} &= 2\mathcal{T}_{4\Phi} + \mathcal{T}'_{4\Phi},
\end{aligned}
\tag{55}
$$

and $\mathcal{T}'_4$ is obtained from $\mathcal{T}_4$ by interchanging y_1 and y_3. Then we have

$$
\begin{aligned}
\mathcal{T}_{4\Psi} &= x_3 K_1(1 + y_2/\bar{y}_1) + 2\bar{x}_3\tilde{K}_1 \\
&\quad + 2x_3(\tilde{K}_2 - K_2) - K_3/\bar{y}_1 \\
&\quad + x_3(K_4 + K_5)/\bar{x}_1 + 2(\tilde{K}_4 + \tilde{K}_5), \\
\mathcal{T}_{4\Phi} &= \mathcal{T}_{4\Psi}(1 \leftrightarrow 3),
\end{aligned}
\tag{56}
$$

where the functions K_i and $\tilde{K}_i$ are defined as

$$K_1 = \frac{1}{x_1 x_3^2 y_1 y_3^2 \bar{x}_1^2 \bar{y}_1}, \qquad K_2 = \frac{1}{x_1 x_2 x_3^2 y_2 y_3^2 \bar{x}_2 \bar{y}_2},$$

$$K_3 = \frac{1}{x_1 x_2 y_1 y_2 \bar{x}_1^2 \bar{y}_1}, \qquad K_4 = \frac{1}{x_1 x_3^2 y_1 y_3 \bar{x}_1 \bar{y}_1^2},$$

$$K_5 = \frac{1}{x_1 x_2 x_3 y_1 y_2 \bar{x}_1 \bar{y}_1^2}, \qquad \tilde{K}_i = K_i (1 \leftrightarrow 3). \tag{57}$$

As mentioned above, the twist-four distribution amplitudes can come from both initial and final-state nucleons. Because of the symmetric property of the partonic scattering amplitudes, these two contributions are the same and have been included in the above final result.

Equations (53) and (46) are the final results of our analysis. Comparing these two, we find that the twist-four contribution is suppressed in $1/t$ but enhanced at the threshold. These two features can be used to disentangle their contributions in experiments. If we limit our discussions in the threshold region, the only contribution comes from the twist-four term.

VI. INTERPRETATION IN TERMS OF GRAVITATIONAL FORM FACTOR?

As mentioned in the Introduction, the near threshold heavy quarkonium production has been argued to provide a direct access to the gluonic gravitational form factors of the nucleon. From the results in previous sections, we have calculated the near threshold photoproduction of heavy quarkonium on the nucleon target at large momentum transfer. The gluonic form factors at large $(-t)$ have been recently calculated in Ref. [55]. We conclude that there is no direct connection between them.

A. Construction of the gluonic operator

The above conclusion can be understood from a detailed analysis of the photon-quarkonium transition amplitude. As discussed in Sec. II, this amplitude can be simplified in the heavy quark mass limit, $M_V^2 \gg (-t)$,

$$\mathcal{M}_\psi^{\mu\nu} = N_\psi \epsilon_\psi^* \cdot \epsilon_\gamma \frac{k_{\gamma,\alpha} k_{\gamma,\beta}}{k_1 \cdot k_\gamma k_2 \cdot k_\gamma} \mathcal{W}_T^{\alpha\beta\mu\nu}. \tag{58}$$

Here, we only keep the leading term in this limit. For simplicity, we have also dropped the associated color factors associated with the t-channel gluons. In the above, $\mathcal{W}_T^{\alpha\beta\mu\nu}$ is defined as

$$\mathcal{W}_T^{\alpha\beta\mu\nu} = -k_1^\alpha k_2^\beta g^{\mu\nu} - k_1 \cdot k_2 g^{\alpha\mu} g^{\beta\nu} + k_1^\nu k_2^\beta g^{\alpha\mu} + k_2^\mu k_1^\alpha g^{\beta\nu}, \tag{59}$$

which can be identified as gluonic operator of $F^\alpha_{\ \rho} F^{\beta\rho}$ acting on the nucleon state. However, the complete scattering amplitude involves the integral of the momenta k_1 and k_2 with the associated propagators depending on them. In

the end, the $\gamma N \to J/\psi N'$ amplitude can be schematically written as

$$\mathcal{A} = N_\psi \epsilon_\psi^* \cdot \epsilon_\gamma \int d^4 k_1 d^4 k_2 \frac{k_{\gamma,\alpha} k_{\gamma,\beta}}{(k_1 \cdot k_\gamma - i\varepsilon)(k_2 \cdot k_\gamma - i\varepsilon)}$$
$$\times \int d^4 \eta_1 d^4 \eta_2 e^{ik_1 \cdot \eta_1 + ik_2 \cdot \eta_2} \langle N'| F^{a,\alpha}_{\ \ \rho}(\eta_1) F^{a,\beta\rho}(\eta_2) |N\rangle. \tag{60}$$

Due to the explicit k_1 and k_2 dependence in the prefactor of $\frac{1}{(k_1 \cdot k_\gamma - i\varepsilon)(k_2 \cdot k_\gamma - i\varepsilon)}$, the above equation cannot be identified as a gluonic gravitational form factor of the nucleon state directly. This prefactor comes from the quark propagators in the photon-quarkonium transition amplitude as we showed in Sec. II. Of course, the complete calculation will have a full dependence on the momentum fractions of the incoming nucleon p_1 carried by the two gluons k_1 and k_2. However, with certain approximations similar to those discussed in Refs. [26,29], the above amplitude can be written in terms of the gluonic gravitational form factors. In the sense, there exists an indirect connection between them.

B. Comparison to the GPD formalism

It is interesting to find out that the above $\mathcal{W}_T^{\mu\nu}$ can be directly compared to that for the gluon GPD calculations. Gluon GPD is defined through the matrix element $\langle N'| F^{+\alpha} F^+_\alpha |N\rangle$. The amplitude associated with this can be written as

$$-n \cdot k_1 n \cdot k_2 g^{\mu\nu} - n^\mu n^\nu k_1 \cdot k_2 + n^\mu k_1^\nu n \cdot k_2 + n^\nu k_2^\mu n \cdot k_1, \tag{61}$$

where n is the light-cone vector used in the GPD definition with $n \cdot k = k^+$ for any momentum k. Here, k_1 and k_2 represent the gluon momenta that couple to the nucleon state, and $\mu\nu$ for their polarization indices. Clearly, this is the same structure as $\mathcal{W}_T^{\mu\nu}$ of the previous subsection if we identify $n \propto k_\gamma$.

Following this argument, the scattering amplitude of $\gamma N \to J/\psi N'$ can be formulated in terms of the gluon GPDs [6,7,9,18,26,29]:

$$\mathcal{A} = N_\psi \epsilon_\psi^* \cdot \epsilon_\gamma \int_{-1}^1 dx \frac{1}{(x + \xi - i\varepsilon)(x - \xi + i\varepsilon)}$$
$$\times \frac{1}{\bar{P}^+} \int \frac{d\eta^-}{2\pi} e^{ix\bar{P}^+\eta^-} \langle N'| F^{a,+}_{\ \ \alpha}\left(-\frac{\eta^-}{2}\right) F^{a,\alpha+}\left(\frac{\eta^-}{2}\right) |N\rangle, \tag{62}$$

where the last factor defines the associated gluon GPDs. In previous sections, we have given explicit examples that demonstrate the consistency between our calculations with the GPD formalism.

Clearly, from the above GPD formalism, one can only link to the gluonic gravitational form factors by making

approximations of no x dependence in the prefactor $\frac{1}{(x+\xi-i\varepsilon)(x-\xi+i\varepsilon)}$ [26,29]. This is the same as we discussed in the previous subsection.

VII. PHENOMENOLOGY APPLICATIONS AND PREDICTIONS FOR ψ' AND Υ FOR FUTURE EXPERIMENTS

The phenomenoloical application of the above derivation to the GlueX data has been carried out in our previous paper [65]. In particular, the twist-four contribution is fitted to the GlueX data [16] with the following parametrization of the differential cross section:

$$\frac{d\sigma}{dt}\Big|^{\text{twist}-4} = \frac{N_0}{(-t+\Lambda^2)^5}, \tag{63}$$

where $\Lambda^2 = 1.41 \pm 0.20 \,\text{GeV}^2$ and $N_0 = 51 \pm 22\,\text{nb} * \text{GeV}^8$. The current data from the GlueX can be well described by the above parametrization. In the following, we will apply this result to the future experiments for the threshold photoproduction of ψ' and Υ.

We have also made an order of magnitude estimate of the differential cross section by applying the twist-four contribution of Eq. (53) with model assumptions for the twist-three and twist-four distribution amplitudes of the nucleon [61,62]. There have been great efforts to compute these distribution amplitudes from various methods [53,68–85], including the lattice QCD, the light-cone sum rule, and model calculations. The differential cross sections calculated from the distribution amplitudes with realistic model assumptions, e.g., those from Ref. [76], are consistent with the experimental data around $-t = 1.5 \,\text{GeV}^2$ and the fitted result of Eq. (63),[1] whereas the results from the asymptotic distribution amplitudes are an order of magnitude smaller.

A. Predictions for ψ' and $\Upsilon(\text{nS})$ production

Extending our analysis to other heavy quarkonium states is straightforward and similar formulas can be derived. As a first step, we take the differential cross section from the twist-four contribution at the threshold,

$$\frac{d\sigma(\gamma p \to Vp)}{dt}\Big|_{\text{threshold}} = \frac{N_0^V}{(-t+\Lambda^2)^5}, \tag{64}$$

for a heavy quarkonium state V. In the heavy quark mass limit, the t dependence only comes from the nucleon side. Therefore, we will assume the above Λ parameter should be the same for all heavy quarkonium states. On the other hand, the normalization factor N_0^V will depend on the

FIG. 7. Differential cross sections for J/ψ and ψ' photoproduction as functions of the momentum transfer t and the total cross sections near the threshold as functions of $W_{\gamma p}$.

quarkonium state in the final state. From the derivations in the previous section, we know that the differential cross section is proportional to

$$\frac{d\sigma}{dt} \propto \frac{\alpha_s^2(M_V)\langle 0|\mathcal{O}^V({}^3S_1^{(1)})|0\rangle}{M_V^7}, \tag{65}$$

from which we derive the ratio between different heavy quarkonium states,

$$\frac{N_0^V}{N_0} = \frac{\alpha_s^2(M_V)\langle 0|\mathcal{O}^V({}^3S_1^{(1)})|0\rangle/M_V^7}{\alpha_s^2(M_\psi)\langle 0|\mathcal{O}^\psi({}^3S_1^{(1)})|0\rangle/M_\psi^7}. \tag{66}$$

Substituting the associated NRQCD matrix elements for J/ψ, ψ', and Υ (1S, 2S) from, e.g., Refs. [86,87], we find the following values for the normalization factors:

$$N_0^{\psi'} = 0.20 N_0, \tag{67}$$

$$N_0^{\Upsilon(1S)} = 5 \times 10^{-3} N_0, \tag{68}$$

$$N_0^{\Upsilon(2S)} = 2.5 \times 10^{-3} N_0. \tag{69}$$

In Fig. 7, we show the threshold cross sections for $\gamma p \to \psi' p$. As comparison, we also show the results for J/ψ. For Upsilon production, the results are plotted in Fig. 8.

The comparison between different quarkonium states will provide an important confirmation for the production

FIG. 8. The differential cross sections for $\Upsilon(1S)$ and $\Upsilon(2S)$ photoproduction as functions of the momentum transfer t and the total cross sections as functions $W_{\gamma p}$ near the threshold.

---

[1]In the numeric calculation of the $G_{p4}(t)$ in Eq. (54), a lower cutoff $[(\sim (0.17\,\text{GeV})^2/(-t)]$ on the momentum fractions x_i and y_i in the integral is imposed to avoid the end-point singularity. This is similar to the Pauli form-factor calculation at large momentum transfer in Ref. [54].
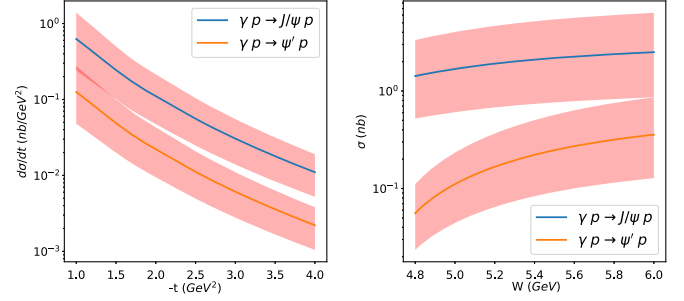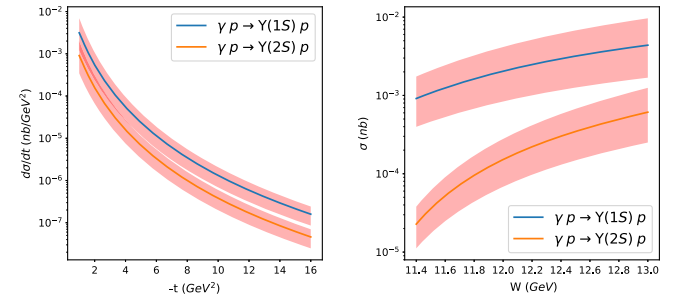
mechanism. The comparison between Charmonium and Bottomonium, in particular, will test the heavy quark limit we have employed in this paper. Meanwhile, the momentum transfer range is much higher for Υ as compared to J/ψ. This provides a unique opportunity to explore the large momentum transfer region.

VIII. CONCLUSION

In this paper, we have carried out a detailed derivation of near threshold heavy quarkonium photoproduction at large momentum transfer. We have taken into account the three-quark Fock state of the nucleon with zero and one unit of quark OAM. We found that the contribution from the Fock state with zero-quark OAM is suppressed at threshold. The differential cross section is dominated by the contribution from nonzero OAM Fock state and has a power behavior of $1/(-t)^5$.

Our power counting predictions are consistent with recent experimental data of near threshold photoproduction of J/ψ from the GlueX collaboration at JLab. Based on the comparison between our derivation and the experimental data, we have made predictions for ψ' and $\Upsilon(1S, 2S)$. All these predictions can be tested at future facilities including the electron-ion colliders [45–47].

Although there is no direct connection between the near threshold photoproduction of heavy quarkonium state and the gluonic gravitational form factors, an indirect connection can be built through GPD gluon distributions. For example, we can parametrize the gluon GPDs and fit to the experimental data, which, in return, can constrain the associated gravitational form factors.

ACKNOWLEDGMENTS

APPENDIX A: GLUON GPD FOR PION

The gluon GPD for pion is defined as

$$
\int \frac{d\eta^-}{2\pi} e^{ix\bar{P}^+\eta^-} \langle p_2|F_a^{+\mu}\left(-\frac{\eta^-}{2}\right)\mathcal{L}_{ab}\left[-\frac{\eta^-}{2},\frac{\eta^-}{2}\right]F_{\mu,b}^+\left(\frac{\eta^-}{2}\right)|p_1\rangle
$$
$$
= \bar{P}^+ H_g^{(\pi)}(x,\xi,t), \tag{A1}
$$

where the gluon field strength tensor is $F_{\mu\nu}^a = \partial_\mu A_\nu^a - \partial_\nu A_\mu^a - g_s f^{abc} A_\mu^b A_\nu^c$, and the gauge link in the adjoint representation is

$$
\mathcal{L}_{ab}[z_2,z_1] = \mathcal{P}\exp\left[g_s \int_{z_1}^{z_2} dz^- G^{+,c}(z^-)f^{acb}\right]. \tag{A2}
$$

$\mathcal{P}$ denotes the path-ordering operation. In the definition of GPD, $\bar{P} = (p_1 + p_2)/2$ is the average momentum, $\Delta = p_2 - p_1$ is the momentum transfer, and $t = \Delta^2$. The skewness parameter ξ is defined as the projection of the momentum transfer Δ along $\bar{P}$ direction, $\xi = -\frac{\Delta^+}{2\bar{P}^+}$.

In the large $(-t)$ limit, the gluon GPD of the pion has the following factorization formula:

$$
H_g^{(\pi)}(x,\xi,t) = \int dx_1 dy_1 \phi(y_1)\phi(x_1)\mathcal{H}^{(\pi)}(x_1,y_1), \tag{A3}
$$

where ϕ represents the leading-twist distribution amplitude of pion. The perturbative function at the leading order can be written as

$$
\begin{aligned}
\mathcal{H}^{(\pi)}(x_1,y_1) = \frac{g_s^2 C_F}{-t}&\left(\frac{(1-\xi)^2}{x_1\bar{x}_1}+\frac{(1+\xi)^2}{y_1\bar{y}_1}\right)\\
&\times (\delta[x - (x_1 - y_1 + \xi(x_1 + y_1 - 1))]\\
&+ \delta[x + (x_1 - y_1 + \xi(x_1 + y_1 - 1))]).
\end{aligned} \tag{A4}
$$

The above result is similar to that of the quark GPD calculated in Ref. [66] for the pion.

APPENDIX B: GLUON GPD FOR NUCLEON

The gluon GPD of nucleon is defined from

$$
\begin{aligned}
&\int \frac{d\eta^-}{2\pi} e^{ix\bar{P}^+\eta^-} \langle p_2, s'|F_a^{+\mu}\left(-\frac{\eta^-}{2}\right)\mathcal{L}_{ab}\left[-\frac{\eta^-}{2},\frac{\eta^-}{2}\right]\\
&\quad \times F_{\mu,b}^+\left(\frac{\eta^-}{2}\right)|p_1, s\rangle\\
&= \frac{1}{2}\left(H_g(x,\xi,t)\bar{U}(p_2,s')\gamma^+ U(p_1,s)\right.\\
&\left.\quad + E_g(x,\xi,t)\bar{U}(p_2,s')\frac{i\sigma^{+\alpha}\Delta_\alpha}{2M_p}U(p_1,s)\right),
\end{aligned} \tag{B1}
$$

where s^μ denotes the covariant spin vector of the proton.

Following the strategy in [55,66], the GPD H_g can be extracted from the helicity-conserved amplitude, and one can show that at the large momentum transfer H_g follows the following factorization formula:

$$
\begin{aligned}
H_g(x,\xi,t) = \int [dx][dy]\Phi_3^*(y_1,y_2,y_3)&\Phi_3(x_1,x_2,x_3)\\
&\times \mathcal{H}(\{x\},\{y\}),
\end{aligned} \tag{B2}
$$

where Φ_3 is the twist-three proton light-cone amplitude [61], and $\mathcal{H}$ is the hard coefficient and perturbatively calculable. At the leading order, we obtain

$$\mathcal{H}(\{x\},\{y\}) = 2\tilde{\mathcal{H}} + \tilde{\mathcal{H}}(y_1 \leftrightarrow y_3), \qquad (B3)$$

where

$$
\begin{aligned}
\tilde{\mathcal{H}} = \frac{4\pi^2\alpha_s^2 C_B^2}{3t^2}\Bigg\{ &\left(\frac{x_1+y_1+\xi(x_1-y_1)}{\bar{x}_1\bar{y}_1x_1x_3y_1y_3} + \frac{x_1+y_1+\xi(x_1-y_1)}{\bar{x}_1\bar{y}_1x_1x_2y_1y_2}\right) \\
&\times (\delta[x-(x_1-y_1+\xi(x_1+y_1-1))] \\
&+ \delta[x+(x_1-y_1+\xi(x_1+y_1-1))]) \\
&+ \left(\frac{x_3+y_3+\xi(x_3-y_3)}{\bar{x}_3\bar{y}_3x_3x_1y_3y_1} + \frac{x_3+y_3+\xi(x_3-y_3)}{\bar{x}_3\bar{y}_3x_3x_2y_3y_2}\right) \\
&\times (\delta[x-(x_3-y_3+\xi(x_3+y_3-1))] \\
&+ \delta[x+(x_3-y_3+\xi(x_3+y_3-1))])\Bigg\}. \qquad (B4)
\end{aligned}
$$

Similar results for the quark GPDs H_q of the nucleon have been calculated in Ref. [66]. They share the same power behavior at large $(-t)$.

On the other hand, the GPD E_g at large $(-t)$ is calculated from the nucleon helicity-flip amplitude, and the related factorization formula can be written as

$$
\begin{aligned}
E_g(x,\xi,t) = \int [dx][dy]\{&x_3\Phi_4(x_1,x_2,x_3)\mathcal{E}_{\Phi g}(\{x\},\{y\}) \\
&+ x_1\Psi_4(x_2,x_1,x_3)\mathcal{E}_{\Psi g}(\{x\},\{y\})\}\Phi_3(y_1,y_2,y_3), \\
&\qquad\qquad\qquad\qquad\qquad\qquad (B5)
\end{aligned}
$$

where Ψ_4 and Φ_4 are the twist-four distribution amplitude of the proton [62]. $\mathcal{E}_g$ can be written as

$$\mathcal{E}_g = 2\tilde{\mathcal{E}} + \tilde{\mathcal{E}}', \qquad (B6)$$

where $\tilde{\mathcal{E}}'$ is obtained from $\tilde{\mathcal{E}}$ by interchanging y_1 and y_3. The detailed calculation yields

$$
\begin{aligned}
\tilde{\mathcal{E}}_\Psi(\{x\},\{y\}) = \frac{-C_B^2 M_p^2}{12(-t)^3}(4\pi\alpha_s)^2[&x_3 K_1\tilde{\delta}[x_1,y_1]((1+\xi)^2 x_1\bar{x}_1 + 2(1-\xi^2)y_3\bar{x}_1 + (1-\xi)^2 y_1 y_2) \\
&+ \bar{x}_3\tilde{K}_1\tilde{\delta}[x_3,y_3]((1+\xi)^2 x_3\bar{x}_3 + (1-\xi)^2 y_3\bar{y}_3) + x_3(\tilde{K}_2 - K_2)\tilde{\delta}[x_2,y_2] \\
&\times ((1+\xi)^2 x_2\bar{x}_2 + (1-\xi)^2 y_2\bar{y}_2) + K_3\tilde{\delta}[x_1,y_1](2(1-\xi^2)\bar{x}_1 - (1-\xi)^2 y_1) + x_3(K_4 + K_5) \\
&\times \tilde{\delta}[x_1,y_1](2(1-\xi^2)\bar{y}_1 + (1+\xi)^2 x_1) + (\tilde{K}_4 + \tilde{K}_5)\tilde{\delta}[x_3,y_3]((1+\xi)^2 x_3\bar{x}_3 + (1-\xi)^2 y_3\bar{y}_3)] + (\xi \leftrightarrow -\xi), \\
&\qquad\qquad\qquad\qquad\qquad\qquad\qquad\qquad\qquad\qquad\qquad\qquad\qquad\qquad\qquad\qquad (B7)
\end{aligned}
$$

and $\tilde{\mathcal{E}}_\Phi = \tilde{\mathcal{E}}_\Psi(1 \leftrightarrow 3)$. Here we have used the following notation to express the delta function of x:

$$\delta[\tilde{a},b] \equiv \delta[x-(a-b+\xi(a+b-1))] + \delta[x+(a-b+\xi(a+b-1))]. \qquad (B8)$$

The functions K_i are the same as those defined in Eq. (57).

[1] M. G. Ryskin, Z. Phys. C **57**, 89 (1993).
[2] S. J. Brodsky, L. Frankfurt, J. F. Gunion, A. H. Mueller, and M. Strikman, Phys. Rev. D **50**, 3134 (1994).
[3] X. D. Ji, Phys. Rev. Lett. **78**, 610 (1997).
[4] X. D. Ji, Phys. Rev. D **55**, 7114 (1997).
[5] J. C. Collins, L. Frankfurt, and M. Strikman, Phys. Rev. D **56**, 2982 (1997).
[6] P. Hoodbhoy, Phys. Rev. D **56**, 388 (1997).
[7] J. Koempel, P. Kroll, A. Metz, and J. Zhou, Phys. Rev. D **85**, 051502 (2012).
[8] Z. L. Cui, M. C. Hu, and J. P. Ma, Eur. Phys. J. C **79**, 812 (2019).
[9] D. Y. Ivanov, A. Schafer, L. Szymanowski, and G. Krasnikov, Eur. Phys. J. C **34**, 297 (2004); **75**, 75(E) (2015).
[10] Z. Q. Chen and C. F. Qiao, Phys. Lett. B **797**, 134816 (2019); **809**, 135759(E) (2020).
[11] C. A. Flett, J. A. Gracey, S. P. Jones, and T. Teubner, J. High Energy Phys. 08 (2021) 150.
[12] D. Kharzeev, Proceedings of the International School of Physics "Enrico Fermi" **130**, 105 (1996).
[13] D. Kharzeev, H. Satz, A. Syamtomov, and G. Zinovjev, Eur. Phys. J. C **9**, 459 (1999).
[14] O. Gryniuk and M. Vanderhaeghen, Phys. Rev. D **94**, 074001 (2016).
[15] Y. Hatta and D. L. Yang, Phys. Rev. D **98**, 074003 (2018).
[16] A. Ali et al. (GlueX Collaboration), Phys. Rev. Lett. **123**, 072001 (2019).
[17] Y. Hatta, A. Rajan, and D. L. Yang, Phys. Rev. D **100**, 014032 (2019).

[18] R. Boussarie and Y. Hatta, Phys. Rev. D **101**, 114004 (2020).

[19] K. A. Mamo and I. Zahed, Phys. Rev. D **101**, 086003 (2020).

[20] O. Gryniuk, S. Joosten, Z. E. Meziani, and M. Vanderhaeghen, Phys. Rev. D **102**, 014016 (2020).

[21] R. Wang, J. Evslin, and X. Chen, Eur. Phys. J. C **80**, 507 (2020).

[22] F. Zeng, X. Y. Wang, L. Zhang, Y. P. Xie, R. Wang, and X. Chen, Eur. Phys. J. C **80**, 1027 (2020).

[23] M. L. Du, V. Baru, F. K. Guo, C. Hanhart, U. G. Meißner, A. Nefediev, and I. Strakovsky, Eur. Phys. J. C **80**, 1053 (2020).

[24] D. E. Kharzeev, Phys. Rev. D **104**, 054015 (2021).

[25] R. Wang, W. Kou, Y. P. Xie, and X. Chen, Phys. Rev. D **103**, L091501 (2021).

[26] Y. Hatta and M. Strikman, Phys. Lett. B **817**, 136295 (2021).

[27] K. A. Mamo and I. Zahed, Phys. Rev. D **103**, 094010 (2021).

[28] W. Kou, R. Wang, and X. Chen, arXiv:2103.10017.

[29] Y. Guo, X. Ji, and Y. Liu, Phys. Rev. D **103**, 096010 (2021).

[30] K. A. Mamo and I. Zahed, Phys. Rev. D **104**, 066023 (2021).

[31] M. A. Shifman, A. I. Vainshtein, and V. I. Zakharov, Phys. Lett. **78B**, 443 (1978).

[32] X. D. Ji, Phys. Rev. Lett. **74**, 1071 (1995).

[33] X. D. Ji, Phys. Rev. D **52**, 271 (1995).

[34] Y. Hatta, A. Rajan, and K. Tanaka, J. High Energy Phys. 12 (2018) 008.

[35] A. Metz, B. Pasquini, and S. Rodini, Phys. Rev. D **102**, 114042 (2020).

[36] Y. Hatta and Y. Zhao, Phys. Rev. D **102**, 034004 (2020).

[37] X. Ji and Y. Liu, Sci. China Phys. Mech. Astron. **64**, 281012 (2021).

[38] X. Ji, Front. Phys. (Beijing) **16**, 64601 (2021).

[39] C. Lorcé, A. Metz, B. Pasquini, and S. Rodini, J. High Energy Phys. 11 (2021) 121.

[40] B. Gittelman, K. M. Hanson, D. Larson, E. Loh, A. Silverman, and G. Theodosiou, Phys. Rev. Lett. **35**, 1616 (1975).

[41] U. Camerini, J. G. Learned, R. Prepost, C. M. Spencer, D. E. Wiser, W. Ash, R. L. Anderson, D. Ritson, D. Sherden, and C. K. Sinclair, Phys. Rev. Lett. **35**, 483 (1975).

[42] S. Joosten and Z. E. Meziani, Proc. Sci. QCDEV2017 (**2018**) 017 [arXiv:1802.02616].

[43] J. Dudek, R. Ent, R. Essig, K. S. Kumar, C. Meyer, R. D. McKeown, Z. E. Meziani, G. A. Miller, M. Pennington, D. Richards et al., Eur. Phys. J. A **48**, 187 (2012).

[44] J. P. Chen et al. (SoLID Collaboration), arXiv:1409.7741.

[45] A. Accardi, J. L. Albacete, M. Anselmino, N. Armesto, E. C. Aschenauer, A. Bacchetta, D. Boer, W. K. Brooks, T. Burton, N. B. Chang et al., Eur. Phys. J. A **52**, 268 (2016).

[46] R. Abdul Khalek, A. Accardi, J. Adam, D. Adamiak, W. Akers, M. Albaladejo, A. Al-bataineh, M. G. Alexeev, F. Ameli, P. Antonioli et al., arXiv:2103.05419.

[47] D. P. Anderle, V. Bertone, X. Cao, L. Chang, N. Chang, G. Chen, X. Chen, Z. Chen, Z. Cui, L. Dai et al., Front. Phys. (Beijing) **16**, 64701 (2021).

[48] G. P. Lepage and S. J. Brodsky, Phys. Rev. Lett. **43**, 545 (1979); **43**, 1625(E) (1979).

[49] S. J. Brodsky and G. P. Lepage, Phys. Rev. D **24**, 2848 (1981).

[50] A. V. Efremov and A. V. Radyushkin, Phys. Lett. **94B**, 245 (1980).

[51] V. L. Chernyak and A. R. Zhitnitsky, JETP Lett. **25**, 510 (1977).

[52] V. L. Chernyak and A. R. Zhitnitsky, Sov. J. Nucl. Phys. **31**, 544 (1980).

[53] V. L. Chernyak and A. R. Zhitnitsky, Phys. Rep. **112**, 173 (1984).

[54] A. V. Belitsky, X. d. Ji, and F. Yuan, Phys. Rev. Lett. **91**, 092003 (2003).

[55] X. B. Tong, J. P. Ma, and F. Yuan, Phys. Lett. B **823**, 136751 (2021).

[56] G. T. Bodwin, E. Braaten, and G. P. Lepage, Phys. Rev. D **51**, 1125 (1995); **55**, 5853(E) (1997).

[57] S. J. Brodsky and G. R. Farrar, Phys. Rev. Lett. **31**, 1153 (1973).

[58] V. A. Matveev, R. M. Muradian, and A. N. Tavkhelidze, Lett. Nuovo Cimento **7**, 719 (1973).

[59] X. d. Ji, J. P. Ma, and F. Yuan, Eur. Phys. J. C **33**, 75 (2004).

[60] L. Frankfurt and M. Strikman, Phys. Rev. D **66**, 031502 (2002).

[61] V. M. Braun, S. E. Derkachov, G. P. Korchemsky, and A. N. Manashov, Nucl. Phys. **B553**, 355 (1999).

[62] V. Braun, R. J. Fries, N. Mahnke, and E. Stein, Nucl. Phys. **B589**, 381 (2000); **B607**, 433 (2001).

[63] X. d. Ji, J. P. Ma, and F. Yuan, Nucl. Phys. **B652**, 383 (2003).

[64] S. J. Brodsky, E. Chudakov, P. Hoyer, and J. M. Laget, Phys. Lett. B **498**, 23 (2001).

[65] P. Sun, X. B. Tong, and F. Yuan, Phys. Lett. B **822**, 136655 (2021).

[66] P. Hoodbhoy, X. d. Ji, and F. Yuan, Phys. Rev. Lett. **92**, 012003 (2004).

[67] G. P. Lepage and S. J. Brodsky, Phys. Rev. D **22**, 2157 (1980).

[68] B. L. Ioffe, Nucl. Phys. **B188**, 317 (1981); **B191**, 591 (1981).

[69] Y. Chung, H. G. Dosch, M. Kremer, and D. Schall, Nucl. Phys. **B197**, 55 (1982).

[70] V. L. Chernyak and I. R. Zhitnitsky, Nucl. Phys. **B246**, 52 (1984).

[71] I. D. King and C. T. Sachrajda, Nucl. Phys. **B279**, 785 (1987).

[72] V. L. Chernyak, A. A. Ogloblin, and I. R. Zhitnitsky, Sov. J. Nucl. Phys. **48**, 536 (1988).

[73] V. L. Chernyak, A. A. Ogloblin, and I. R. Zhitnitsky, Yad. Fiz. **48**, 1410 (1988).

[74] J. Bolz and P. Kroll, Z. Phys. A **356**, 327 (1996).

[75] V. M. Braun, A. Lenz, N. Mahnke, and E. Stein, Phys. Rev. D **65**, 074011 (2002).

[76] V. M. Braun, A. Lenz, and M. Wittmann, Phys. Rev. D **73**, 094019 (2006).

[77] M. Gockeler, R. Horsley, T. Kaltenbrunner, Y. Nakamura, D. Pleiter, P. E. L. Rakow, A. Schafer, G. Schierholz, H. Stuben, N. Warkentin et al., Phys. Rev. Lett. **101**, 112002 (2008).

[78] V. M. Braun, A. N. Manashov, and J. Rohrwild, Nucl. Phys. **B807**, 89 (2009).

[79] V. M. Braun *et al.* (QCDSF Collaboration), Phys. Rev. D **79**, 034504 (2009).

[80] K. Passek-Kumericki and G. Peters, Phys. Rev. D **78**, 033009 (2008).

[81] A. Lenz, M. Gockeler, T. Kaltenbrunner, and N. Warkentin, Phys. Rev. D **79**, 093007 (2009).

[82] I. V. Anikin, V. M. Braun, and N. Offen, Phys. Rev. D **88**, 114021 (2013).

[83] V. M. Braun, S. Collins, B. Gläßle, M. Göckeler, A. Schäfer, R. W. Schiel, W. Söldner, A. Sternbeck, and P. Wein, Phys. Rev. D **89**, 094511 (2014).

[84] G. S. Bali, V. M. Braun, M. Göckeler, M. Gruber, F. Hutzler, A. Schäfer, R. W. Schiel, J. Simeth, W. Söldner, A. Sternbeck *et al.*, J. High Energy Phys. 02 (2016) 070.

[85] G. S. Bali *et al.* (RQCD Collaboration), Eur. Phys. J. A **55**, 116 (2019).

[86] Y. Feng and J. X. Wang, Adv. High Energy Phys. **2015**, 1 (2015).

[87] X. J. Zhan and J. X. Wang, Chin. Phys. C **45**, 023112 (2021).